SAE Technical Paper Series, January 2026, Article number 5027
DOI: 10.4271/2026-01-5027

Enhancing the Aerodynamic Performance of Diffusers in High-performance Vehicles Using Trapped Vortex Cavities

Ming Kin Ng, Tom-Robin Teschner

Cranfield University

(Dated: April 19, 2026)

Motivated by the inclusion of active flow control provisions in the 2026 Formula One regulations, and building upon previous studies of Trapped Vortex Cavity (TVC) implementation in inverted front wings, this paper investigates the effectiveness of TVC as a flow control mechanism applied to vehicle diffusers. Both active and passive configurations were considered for three diffuser geometries: a base straight-line diffuser, an inverted airfoil-shaped diffuser, and a diffuser inspired by a Formula One car. The study employed numerical simulations to evaluate the aerodynamic performance and the potential benefits of integrating TVC systems. Across all types of diffusers, the implementation of a circular TVC cavity resulted in a significant improvement in the lift-to-drag ratio (C_L/C_D). In the active flow control configuration, a 10% improvement was observed in the straight diffuser under a limited mass flow rate. With optimized cavity positioning and radius, the airfoil-shaped and Formula One inspired diffusers achieved improvements of 38.9% and 54.6%, respectively, under the same flow conditions. Passive flow control also demonstrated notable aerodynamic benefits without additional energy input. Compared to the original diffuser configurations, performance gains of 8%, 23.6%, and 12.9% were recorded for the straight, airfoil-shaped, and Formula One inspired diffusers, respectively. The results suggest that the integration of a TVC system in the diffuser could effectively enhance aerodynamic performance by strengthening suction effects and promoting secondary pressure recovery, regardless of diffuser geometry.

Keywords: Trapped Vortex Cavities, Aerodynamics performance, Diffusers

NOMENCLATURE

Parameter Notation	Definition	Unit
TVC	Trapped Vortex Cavity	–
FIA	Fédération Internationale de l'Automobile	–
$F1$	Formula One	–
CFD	Computational Fluid Dynamics	–
DRS	Drag Reduction System	–
C_L	Lift coefficient	–
C_D	Drag coefficient	–
$C_{L_{\text{extrapolated}}}$	Richardson extrapolated value for lift coefficient	–
$C_{D_{\text{extrapolated}}}$	Richardson extrapolated value for drag coefficient	–
C_L/C_D	Lift-to-drag ratio	–
$\dot{m}_{\text{in}}$	Mass flow rate	kg/s
ρ	Air density	kg/m^3
A	Cross-sectional area	m^2
V_{in}	Velocity of flow entering the cavity	m/s
V_∞	Freestream velocity	m/s
h_{in}	Height of passive tunnel inlet	m
h_{out}	Height of passive tunnel outlet	m
N_{cells}	Number of cells	–
D_{TVC}	Diameter of Trapped Vortex Cavity	m
L_{diff}	Straight-line distance of diffuser	m
GCI	Grid Convergence Index	–
$GCI_{\text{asymptotic}}$	Asymptotic range	–
r	Refinement ratio	–
p	Order of accuracy	–

Published by SAE. This is the Author Accepted Manuscript issued with: Creative Commons Attribution License (CC:BY 4.0).
The final published version (version of record) is available online at DOI:10.4271/2026-01-5027. Please refer to any applicable publisher terms of use.

I. INTRODUCTION

This paper investigates the effectiveness of the Trapped Vortex Cavity (TVC) concept when integrated into rear diffuser geometries, with the aim of enhancing aerodynamic performance through both active and passive flow control strategies. The study builds upon previous work involving TVC implementation on Formula One front wings [1], extending the concept to the vehicle underbody. The research is also informed by the upcoming 2026 regulations introduced by the Fédération Internationale de l'Automobile (FIA), which are expected to permit active aerodynamic systems in Formula One competition. This regulatory opens new opportunities to re-evaluate active flow control technologies such as TVC within high-performance motorsport applications.

The Trapped Vortex Cavity (TVC) concept is based on the formation of a stable recirculating vortex within a cavity near the separation region on the suction side of an airfoil. Anchoring the vortex inside the cavity energizes the surrounding flow and encourages it to reattach downstream, thereby delaying flow separation. This mechanism has been previously applied to the front wing of a Formula One vehicle, where the integration of TVC with active flow control demonstrated an improvement in lift-to-drag ratio (C_L/C_D) [1]. A higher C_L/C_D contributes to enhanced aerodynamic efficiency by increasing downforce while minimizing the associated drag penalty. However, focusing aerodynamic development solely on the front axle can result in an imbalance in load distribution, leading to increased pitch shift at high speeds. This forward pitch, particularly during cornering at the limit of tire grip, may induce oversteer or even vehicle instability, ultimately compromising performance and driver control.

Achieving a well-balanced front-to-rear aerodynamic load is, therefore, essential for ensuring stable handling, improved traction, and overall race competitiveness. This is especially critical on demanding circuits such as the Monaco Grand Prix, where precise aerodynamic balance contributes not only to vehicle stability but also to higher cornering speeds and the ability to maintain closer racing distances — potentially increasing overtaking opportunities on subsequent straights. With a well-balanced aerodynamic package, the overall benefit can lead to a lap time reduction of approximately $t = 1$ s [2].

The diffuser, integrated with the underbody geometry of a Formula One vehicle, plays a critical role in aerodynamic performance, rounding to 61.09% of the total downforce [3]. Similarly to the front wing, the diffuser enhances the downforce by increasing the suction effect beneath the vehicle. Diffuser , as shown in Figure 1, consists of a single diverging ramp section at the rear of the underfloor. When high-speed airflow travels beneath the flat floor of the car, the diffuser facilitates a gradual expansion of this flow as it transitions to the ambient freestream at the vehicle's rear. This gradual expansion reduces the flow velocity and enables partial pressure recovery at the diffuser exit. Meanwhile, the diverging geometry further lowers the static pressure at the inlet region, effectively acting as a passive flow acceleration mechanism. The pressure differential between the low-pressure inlet and the higher-pressure outlet enhances the aerodynamic loading on the underbody, thereby increasing the total downforce generated. The combination of a strong suction peak at the diffuser inlet and a favorable pressure gradient toward the rear makes the diffuser a key component in maximizing rear-end aerodynamic efficiency.

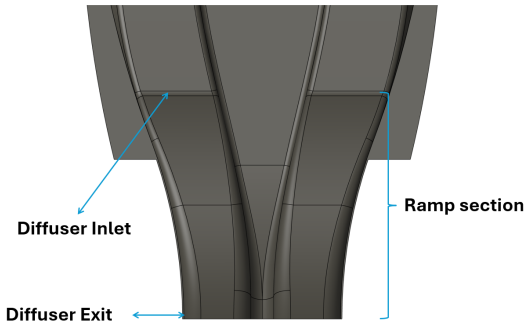

Figure 1: Diffuser section of the baseline Formula One model inspired in the study

To further improve the aerodynamic performance of the diffuser, the Trapped Vortex concept is proposed as a potential method for enhancing the C_L/C_D in the rear underbody region. The TVC system is implemented along the diffuser surface to increase the suction effect and enable a more effective pressure recovery toward the outlet. In addition, a more substantial adverse camber effect is expected to be promoted, contributing to improved flow curvature and a reduction in the size of the wake region behind the vehicle. These modifications are intended to enhance rear-end downforce while avoiding a significant increase in aerodynamic drag.

This paper investigates the aerodynamic performance of a diffuser equipped with a TVC system using both active and passive flow control methods based on numerical simulations. The study begins with a literature review covering previous efforts to enhance diffuser efficiency and the application of TVC technology within the motorsport domain. A baseline diffuser with a straight-line

design is first analyzed to establish a reference and validate the approach. Subsequently, the TVC is integrated into an airfoil-shaped and Formula One inspired diffuser to assess and optimize the C_L/C_D. The objective is to identify the most effective configuration and placement of TVC for maximizing aerodynamic performance under racing conditions.

II. LITERATURE REVIEW

Active flow control refers to the injection of energy into an airflow to manipulate flow separation [4]. One of the earliest applications of active flow control in motorsports was demonstrated by the *Chaparral 2J* in 1970, in which a rear-mounted fan was employed to extract air from beneath the vehicle, thereby generating a low-pressure region and increasing downforce [5]. However, as identified by Maciej et al. [6], such fan-driven systems were found to produce turbulent, dust-laden airflow that negatively affected trailing vehicles. This limitation led to the system being prohibited under FIA regulations. In contemporary Formula One, the Drag Reduction System (DRS) is regarded as a more controlled and regulated form of active flow control. Through the adjustment of the rear wing flap angle, pressure drag is reduced, allowing for increased straight-line velocity during overtaking maneuvers. Despite its effectiveness in such scenarios, studies have reported a downforce reduction exceeding 113% on the flap element and approximately 39% across the rear wing as a whole [7], thereby constraining its utility in cornering conditions.

Due to strict FIA regulations restricting active flow control and fixed geometric boundaries for ramp angle and ride height, research on open-wheel racecar diffuser performance has primarily focused on passive aerodynamic strategies, particularly through geometric modifications. Among these, optimizing the curvature of the diffuser ramp has been shown to delay flow separation and promote reattachment. By introducing an asymmetric, curved surface toward the aft section, a stronger suction peak can be generated at the diffuser inlet, enhancing underbody pressure gradients and improving aerodynamic efficiency. This principle was first exemplified in the *Lotus 78* and *Lotus 79* [8], which utilized inverted airfoil-shaped underbodies to exploit ground effect and enhance underbody suction. In more recent work, the concept of a curved underbody diffuser has been further explored through CFD simulations, ranging from simplified to more complex vehicle models. Angel et al. [9] investigated this approach by integrating a curved diffuser into an Ahmed body, reporting an average increase of 22% in the downforce coefficient compared to a flat diffuser configuration. Building on this foundation, Chatpattanasiri et al. [10] conducted a CFD-based study comparing side-diffuser designs with straight-line and spline-shaped geometries on a Formula SAE vehicle. Their results demonstrated that the curved (spline) diffuser, when designed with an optimal ramp angle, produced significantly more downforce than the flat diffuser under identical conditions. When integrated into the complete vehicle model, the spline diffuser led to a 10% increase in drag but yielded a 30% gain in total downforce.

Apart from diffuser optimization through geometric curvature modifications, Kuya et al. [11] explored using vortex generators to further enhance diffuser performance. Their experimental study on a flat plate configuration demonstrated that vortex generators could stabilize and trap vortices, generating a stronger counter-rotating streamwise vortex pair along the diffuser surface. However, the presence of the devices introduced additional form drag, contributing to an overall increase in total drag. Laura et al. [12] investigated the effect of incorporating vertical airfoil-shaped endplates on a diffuser mounted to an Ahmed body. The endplates were found to generate strong longitudinal vortices, helping to reduce pressure at the rear of the body. This configuration resulted in a substantial 51% increase in downforce, albeit at the cost of a comparable increase in drag, attributed to a more energetic and expanded wake region. Peddie et al. [13] used CFD analysis to optimize the length of the central diffuser in a Formula 3 car, gaining an additional 6% in downforce. However, this improvement was accompanied by a measurable increase in drag compared to a baseline diffuser, highlighting the trade-offs involved in such passive flow control strategies.

A potential future direction to maximize diffuser aerodynamic performance involves implementing flow control techniques that generate a secondary low-pressure region during the pressure recovery region inlet [14]. When combined with a reconsideration attitudes toward limited active flow control strategies from FIA, the Trapped Vortex Cavity (TVC) concept shows particular promise due to its ability to intensify suction effects while simultaneously delaying flow separation.

The trapped vortex concept was first proposed by Ringleb [15] and has demonstrated aerodynamic benefits in airfoil applications. When operated with a constant mass flow rate, active TVC systems can effectively maintain a stable vortex within the cavity, suppress large-scale vortex shedding [16], and reduce drag at low angles of attack [17]. Furthermore, increasing the mass flow rate has been shown to delay stall onset

by over four degrees [18], resulting in a significant improvement in the lift-to-drag ratio compared to clean airfoil configurations.

To evaluate whether the advantages of TVC observed in airfoil research could be translated into ground-effect aerodynamics, the previous study focused on the application of TVC within an inverted front wing configuration [1]. In the work, the TVC was positioned at three locations: the trailing edge of the slat airfoil (softer edge), the mid airfoil (moderate angle of attack), and the flap airfoil (sharper edge with high flap angle). Under active control, a maximum C_L/C_D improvement of up to 313% was achieved when the TVC was implemented on the mid airfoil, relative to the baseline configuration, thereby demonstrating the potential of TVC systems in enhancing ground interaction performance. The results also highlighted the influence of airfoil curvature on TVC effectiveness: a gentler surface curvature amplified the ability of the TVC to suppress wake formation and reduce drag, whereas a sharper curvature, while more prone to separation, allowed for stronger flow acceleration and produced a more pronounced low-pressure region. However, this prior study employed a relatively high mass-flow rate within the cavity, raising concerns about the unquantified energy cost associated with such control strategies. Additionally, when the TVC was implemented in the passive case, a drop in aerodynamic performance was recorded, primarily due to the added drag induced by the internal channel connecting the cavity to the stagnation point of the airfoil and the recirculating region inside the tunnel.

In the present study, TVC is reintroduced as an alternative flow control method to optimize a diffuser's C_L/C_D ratio. The system is integrated into diffuser geometries with varying curvatures to evaluate its effectiveness across different design conditions. A key objective of implementing the TVC is to enhance the suction peak at the diffuser inlet and to generate a secondary pressure recovery region downstream. These effects are targeted based on the TVC's ability to intensify local suction and influence downstream flow behavior. A constrained blowing energy strategy is employed to balance aerodynamic performance with energy efficiency. Furthermore, a redesigned passive configuration is considered, incorporating a lower-drag internal tunnel to minimize the adverse effects observed in earlier implementations.

III. METHODOLOGY

A. Geometry and Cavity design

This study investigates three primary diffuser geometries. The first geometry is a baseline configuration featuring a straight diffuser surface with a chord length of 1.03 m, as illustrated in Figure 2. The second geometry is an inverted airfoil-shaped diffuser, inspired by the design language of the *Lotus 78* and *Lotus 79* [8], and is shown in Figure 3. This configuration shares the same chord length of 1.03 m as the baseline, while the arc length of its curved surface measures 1.034 m. The third geometry draws inspiration from the ramp-style diffuser of a 2022 baseline Formula One model. The original 3D geometry of the aft section is illustrated in Figure 4, and the corresponding cross-sectional profile is shown in Figure 5. It also maintains a chord length of 1.03 m, with an arc length of 1.036 m.

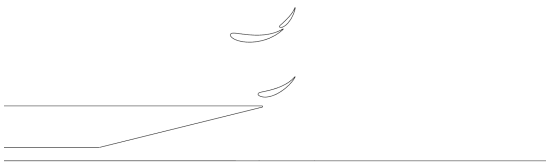

Figure 2: Geometry used in the straight-line diffuser configuration. The model features a straight ramp surface connected to the underbody floor and the diffuser rear section. The geometry also includes the DRS system, represented by a beam wing and a two-element airfoil. All geometric parameters, except for the shape of the ramp surface, remain identical across all simulation cases.

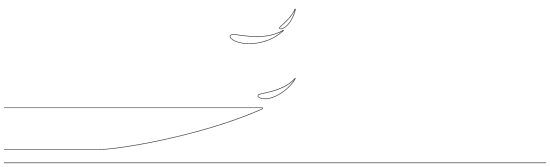

Figure 3: Geometry used in the airfoil-shaped diffuser configuration. The model features a inverted airfoil-shaped ramp surface connected to the underbody floor and the diffuser rear section. The geometry also includes the DRS system, represented by a beam wing and a two-element airfoil. All geometric parameters, except for the shape of the ramp surface, remain identical across all simulation casesr.

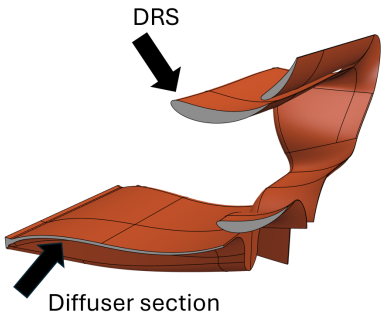

Figure 4: 3D model of the aft part of the baseline Formula One model inspired in the study

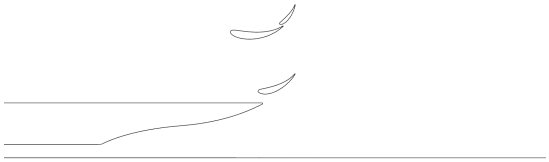

Figure 5: Geometry used in the Formula One inspired diffuser configuration. The model features a Formula One-style ramp surface defined by a cross-sectional curve, as referenced in Figure 4.The geometry also includes the DRS system, represented by a beam wing and a two-element airfoil. All geometric parameters, except for the shape of the ramp surface, remain identical across all simulation cases.

All three diffuser geometries are mounted to the same underbody wall profile and paired with an identical Drag Reduction System (DRS) consisting of a beam wing and a two-element main wing. The chord length of the beam wing is 0.225 m, while the combined chord length of the two-element main wing is 0.4 m.

The diffuser angle and ground clearance are kept constant for all diffuser configurations to eliminate any external variables that could influence aerodynamic performance beyond the effects introduced by diffuser curvature and TVC implementation. This approach ensures that the only parameters varied within each case study are the diffuser surface geometry and the TVC-related variables. By controlling all other factors, the study isolates the impact of these two variables, thereby maintaining a single independent variable in each comparison.

Similar to the cavity features investigated in airfoil configurations [19] and inverted three-element airfoils [1], the cavity integrated into the diffuser in this study adopts a circular shape and the detail feature is illustrated in Figure 6, this geometry gives rise to several critical flow features. These include the *Cusp Point*, where the flow direction reverses and is redirected toward the stagnation region; the *Stagnation Point*, where the flow velocity drops to zero, and the stream divides; and the *Inflection Point*, where the pressure gradient reverses.

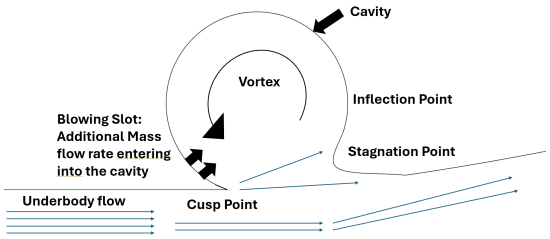

Figure 6: Features of the TVC configuration, with arrows indicating the direction of the underbody flow and the vortex motion within the cavity.

The placement of the TVC varies across the different diffuser configurations to optimize the TVC's locations. The TVC is positioned at the midsection for the base straight-line diffuser, allowing the concept to be evaluated within a geometrically fundamental and straightforward diffuser layout. Multiple cavity locations were investigated for the airfoil-shaped diffuser and the contemporary Formula One inspired diffuser, including placements at the leading edge and mid-chord of the diffuser surface. These configurations were selected to enhance the diffuser's pumping effect and introduce a secondary pressure recovery mechanism, thus improving overall aerodynamic performance.

All diffuser configurations in this study were evaluated at a freestream Reynolds number of 3.4×10^6, corresponding to a velocity of 50 m/s. This operating condition was chosen to reflect the aerodynamic demands typically encountered during high-speed cornering, where achieving a high C_L/C_D is essential. Such corners often lead into overtaking zones, making aerodynamic efficiency particularly critical.

For example, Turn 14 at Suzuka Circuit is taken at an average speed of approximately 175 km/h (48.6 m/s)[20], just before a key overtaking straight. Similarly, at Silverstone Circuit, cars can reach speeds up to 220 km/h (61.1 m/s) through Chapel curve[21], which also precedes a long straight. These cases demonstrate that the selected velocity of 50 m/s falls within a representative range for real-world racing conditions. Furthermore, this velocity is consistent with that used in prior studies [1], facilitating more direct

comparisons—particularly in assessing front–rear aerodynamic balance, a key factor in maximizing traction and handling performance.

B. Active vs. Passive blowing

Both active and passive blowing techniques share a common objective: to supply sufficient momentum to anchor a vortex within the cavity, thereby capturing the incoming flow and enhancing the suction effect. This mechanism helps reattach the ejected flow to the diffuser surface, improving aerodynamic performance. However, the two methods differ fundamentally in their operational approach.

In the active blowing configuration, external energy is required to generate the necessary momentum within the cavity. To implement this, a blowing slot is introduced near the cusp point in all studied geometries, with its length consistently scaled relative to the TVC diameter. To ensure physically realistic mass injection in the active TVC cases, the blowing slot is modeled as the mass-flow inlet boundary condition and the strength of the blowing is governed by the mass-flow rate, defined as:

$$\dot{m}_{\text{in}} = V_{\text{in}} \rho A, \tag{1}$$

Where V_{in} is the velocity of the flow entering the cavity through the blowing slot (normal to the surface), ρ is the air density, and A is the cross-sectional area of the slot.

In this study, the blowing intensity is represented by the non-dimensional ratio V_{in}/V_{∞}, where V_{∞} is the freestream velocity at the inlet. To simulate a realistic and energy-efficient implementation of the TVC system under racecar conditions, all active blowing cases are constrained to a mass-flow rate corresponding to $V_{\text{in}}/V_{\infty} \leq 2$. This limitation ensures that the system remains within practical bounds of energy consumption while still achieving measurable aerodynamic benefits.

In the passive-blowing configuration, no external energy input is required. Instead, a geometric modification is introduced to produce a self-sustained blowing effect. The concept of passive blowing is inspired by the study in [22], where a channel was embedded within an airfoil, extending from the leading edge to the trailing edge. This channel allowed high-pressure air from the stagnation point at the leading edge to feed into the low-pressure wake region, effectively generating a vortex without external energy.

In this study, a similar approach is adapted for the diffuser configuration and therefore a channel is placed near to the diffuser inlet, as introduced in Figure. 7, a passive tunnel is connected to the TVC, enabling ambient-pressure air to be drawn into the low-pressure region within the cavity. This setup aims to generate free-blowing momentum, enhancing vortex strength and aiding flow attachment along the diffuser surface.

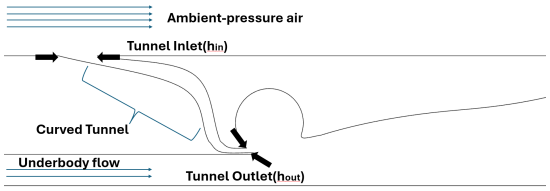

Figure 7: Geometry of the passive tunnel used in this study. The ratio of $h_{\text{in}}/h_{\text{out}}$ is maintained at 5 in all passive cases to achieve optimal performance, as indicated by previous studies.

The tunnel walls are modeled as no-slip boundaries, while the tunnel outlet is directly exposed to the ambient free-stream region. A key governing parameter in the passive mass injection process is the length ratio between the tunnel inlet and outlet heights, h_{in} and h_{out}, which controls the effectiveness of pressure-driven flow entering the cavity. In this study, the inlet-to-outlet ratio, $h_{\text{in}}/h_{\text{out}}$, is fixed at a value of 5. This choice is guided by earlier investigations [1], which demonstrated that a ratio of 5 yields the optimal performance for a NACA0012 airfoil equipped with a TVC system. Accordingly, the same ratio has been adopted for all passive configurations examined in the present work.

Furthermore, unlike the straight tunnel used previously, a curved tunnel design is implemented in the present work. This modification aims to minimize the flow recirculation observed in the straight tunnel configuration, thereby reducing associated drag penalties and improving overall aerodynamic efficiency. However, it is important to note that the internal channel represents an initial design and has not yet undergone optimization. The current configuration includes two nearly 90-degree turning sections, which inherently induce additional pressure drag. Consequently, further refinement of the tunnel geometry will be necessary to mitigate these effects, particularly when the system is transitioned to practical applications.

C. Grid Settings

The computational grids for all diffuser configurations were generated using Fidelity Pointwise.

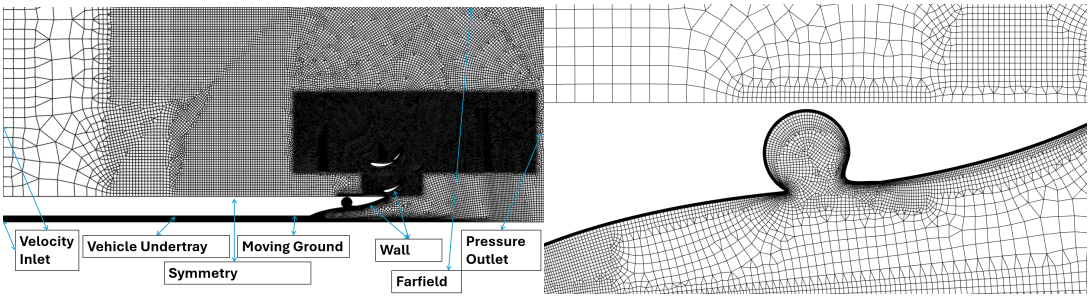

(a) Entire Mesh Domain (b) Zoom into cavity

Figure 8: Mesh domain used in the paper: This configuration represents a simplified design focused on analyzing diffuser aerodynamics. A narrow tunnel is connected downstream of the diffuser to approximate underbody flow conditions, while symmetry boundaries are applied to enable efficient and representative flow simulations.

A wall-resolved approach was employed, with structured quadrilateral elements used in the inflation layer near the wall boundaries. The first cell height was set to achieve $y^+ = 1$, ensuring adequate resolution of the viscous sublayer. A growth rate of 1.2 was applied, with approximately 15 inflation layers used to fully capture the boundary layer development.

In the farfield region, a quad-dominant advancing front technique was used to generate the mesh, incorporating local refinement around the diffuser and DRS geometries to improve solution accuracy. This meshing strategy was applied consistently across all simulation cases to maintain uniformity and ensure reliable comparison of aerodynamic performance.

D. CFD Setup

All simulations were performed using an incompressible flow solver, resolving the Reynolds-Averaged Navier–Stokes (RANS) equations. The pressure–velocity coupling was handled using the SIMPLE algorithm. Turbulence was captured using the k-ω SST model, which provides improved accuracy in capturing adverse pressure gradients and boundary layer separation. To evaluate flow separation across the different configurations, velocity contour plots with consistent scaling were examined to identify recirculation zones and detachment regions. This assessment was further supported by analyzing wall shear stress distributions, from which separation points were inferred based on near-zero shear stress, and by comparing the lift and drag coefficients to quantify the aerodynamic effects of separation.

Convergence was considered achieved when the window-averaged lift and drag coefficients varied by less than 0.1% over a window size of 50 iterations. This criterion ensured both numerical stability and solution consistency across all simulation cases.

E. Boundary condition

The complete mesh domain is illustrated in Figure 8. This configuration represents a preliminary design, primarily intended to investigate the aerodynamic performance solely within the diffuser, rather than modeling the entire rear region of the vehicle, in order to enable a comparative study between different diffuser designs. As shown in the figure, a narrow tunnel is connected downstream to the diffuser. This feature is designed to approximate the underbody flow between the moving ground and the vehicle undertray. The diffuser is also connected to the rear section of the domain and a symmetry boundary, allowing for a simplified yet representative flow behavior.

The inlet boundary condition for all simulations was specified as a velocity inlet. In all cases, the freestream Reynolds number was set to 3.4×10^6. The turbulence intensity was defined as 5%, and the turbulent viscosity ratio was set to 10. At the outlet, a pressure outlet boundary condition was applied with a gauge pressure of 0 Pa.

For the top boundary of the domain, a zero-shear stress condition was imposed to simulate the freestream environment. A moving ground condition was applied at the bottom boundary, with its velocity matched to the inlet freestream velocity to replicate realistic ground effect conditions.

The ramp surface of the diffuser and its associated Drag Reduction System (DRS) were modeled using no-slip wall boundary conditions to accurately capture viscous effects. The same no-slip condition was also applied to the floor and the rear part where it connects to the ramp surface. The slot region was defined as a mass flow inlet, allow-

ing for either active or passive blowing depending on the configuration under investigation.

IV. RESULT AND DISCUSSION

A. Validation

N_{cells}	C_L	r	GCI	$GCI_{\text{asymptotic}}$	p	$C_{L_{\text{extrapolated}}}$
490799	-7.4314e-01	1.46	0.52%			
228964	-7.4537e-01	1.46	0.90%	0.997	1.41	-7.40e-01
107589	-7.4914e-01	-	-			
228964	-7.4537e-01	1.46	0.45%			
107589	-7.4914e-01	1.47	1.08%	1.005	2.32	-7.43e-01
49640	-7.5854e-01	-	-			
N_{cells}	C_D	r	GCI	$GCI_{\text{asymptotic}}$	p	$C_{D_{\text{extrapolated}}}$
490799	1.8260e-01	1.46	0.55%			
228964	1.8316e-01	1.46	0.93%	0.997	1.38	1.82e-01
107589	1.8409e-01	-	-			
228964	1.8316e-01	1.46	0.46%			
107589	1.8409e-01	1.47	1.09%	1.005	2.31	1.82e-01
49640	1.8641e-01	-	-			

Table I: Grid convergence study of C_L and C_D over 4 grids for Straight-line Diffuser

N_{cells}	C_L	r	GCI	$GCI_{\text{asymptotic}}$	p	$C_{L_{\text{extrapolated}}}$
488732	-7.6589e-01	1.46	1.97%			
229132	-7.6929e-01	1.46	2.51%	0.996	0.66	-7.54e-01
107162	-7.7366e-01	-	-			
229132	-7.6929e-01	1.46	0.51%			
107162	-7.7366e-01	1.47	1.21%	1.006	2.31	-7.66e-01
49508	-7.8442e-01	-	-			
N_{cells}	C_D	r	GCI	$GCI_{\text{asymptotic}}$	p	$C_{D_{\text{extrapolated}}}$
488732	1.7606e-01	1.46	3.15%			
229132	1.7692e-01	1.46	3.74%	0.995	0.47	1.72e-01
107162	1.7796e-01	-	-			
229132	1.7692e-01	1.46	0.47%			
107162	1.7796e-01	1.47	1.19%	1.006	2.48	1.76e-01
49508	1.8069e-01	-	-			

Table II: Grid convergence study of C_L and C_D over 4 grids for the Airfoil-shaped Diffuser

N_{cells}	C_L	r	GCI	$GCI_{\text{asymptotic}}$	p	$C_{L_{\text{extrapolated}}}$
475523	-7.8145e-01	1.44	5.40%			
229587	-7.8612e-01	1.47	6.11%	0.994	0.36	-7.48e-01
106714	-7.9172e-01	-	-			
229587	-7.8612e-01	1.47	1.11%			
106714	-7.9172e-01	1.47	1.99%	1.007	1.54	-7.79e-01
49395	-8.0190e-01	-	-			
N_{cells}	C_D	r	GCI	$GCI_{\text{asymptotic}}$	p	$C_{D_{\text{extrapolated}}}$
475523	1.9059e-01	1.44	3.28%			
229587	1.9161e-01	1.47	3.92%	0.994	0.51	1.86e-01
106714	1.9289e-01	-	-			
229587	1.9161e-01	1.47	0.94%			
106714	1.9289e-01	1.47	1.77%	1.007	1.66	1.90e-01
49395	1.9534e-01	-	-			

Table III: Grid convergence study of C_L and C_D over 4 grids for Formula one inspired diffuser

A grid convergence study was conducted for the straight-line diffuser, the airfoil-shaped diffuser, and the Formula One-inspired diffuser, corresponding to the geometries illustrated in Figure 2, Figure 3, and Figure 5, respectively. The objective was to evaluate the lift coefficient (C_L) and drag coefficient (C_D) across coarse, medium, fine and super fine grid resolutions. The mesh configurations for each grid level follow the parameters detailed in the grid setting section. The results of the grid convergence index (GCI) analysis for each diffuser type are presented in Tables I, II, and III.

The number of mesh elements is denoted by N_{cells}, and the refinement ratio between successive grids is represented by r. The extrapolated values of the aerodynamic coefficients, $C_{L,\text{extrapolated}}$ and $C_{D,\text{extrapolated}}$, were estimated using Richardson extrapolation. The Grid Convergence Index (GCI) was computed as a percentage to quantify the discretization uncertainty, with $GCI_{\text{asymptotic}}$ used to evaluate the proximity of the numerical solution to the asymptotic range. The observed order of accuracy, p, was also determined for each case.

The results demonstrate consistent and monotonic convergence behavior across all geometries, confirming the adequacy and reliability of the CFD mesh quality. Based on these findings, the fine mesh resolution was selected for all subsequent simulations, as it provides a balanced trade-off between computational cost and numerical accuracy. This selection ensures sufficient spatial resolution to capture the relevant flow features while minimizing discretization-related uncertainty.

B. Straight-line Diffuser

1. *Active Aerodynamics Case*

A parametric study presented in Figure 9 is conducted to evaluate the overall aerodynamic performance of a straight-line diffuser equipped with a TVC system under varying mass-flow rates. In this study, the TVC diameter is fixed relative to the diffuser length, with a ratio of $D_{\text{TVC}}/L_{\text{diff}} = 0.15$.

The mass-flow rate introduced through the TVC blowing slot is calculated using Equation 1, where V_{in} is the velocity of the flow exiting the slot, as indicated in Figure 6, and V_∞ is the freestream velocity at the diffuser inlet. Their ratio, V_{in}/V_∞, serves as a dimensionless parameter representing the relative strength of the blowing flow.

To assess the aerodynamic impact of the TVC

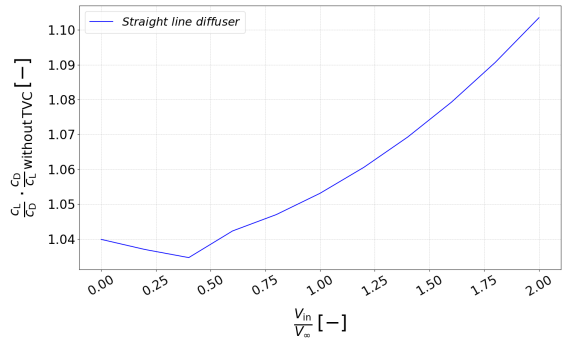

Figure 9: Straight-line Diffuser attached with TVC at mid location with mass-flow rate anachored inside the cavity: $V_{in}/V_{\infty}[-]$ represents the mass-flow rate in term of velocity entering into the cavity versus free-stream velocity; $c_L/c_D[-]$ represent Lift coefficient versus Drag coefficient

system on the straight-line diffuser, C_L/C_D is used as a performance metric. This ratio, calculated for the diffuser equipped with the TVC, is normalized by the corresponding value for a baseline straight-line diffuser without the TVC system. The normalized C_L/C_D is plotted on the y-axis in Figure 9, while the mass-flow rate parameter V_{in}/V_{∞} is shown on the x-axis. A normalized value of 1 indicates that the aerodynamic performance of the TVC-equipped diffuser is equivalent to that of the baseline straight-line diffuser.

The results indicate that within a limited mass-flow range—up to $V_{\text{in}}/V_{\infty} = 2$, the straight-line diffuser equipped with the TVC demonstrates an improvement in aerodynamic performance, as measured by the C_L/C_D ratio. Notably, even at zero mass flow, the diffuser with the TVC achieves a 4% higher C_L/C_D compared to the baseline diffuser without TVC. As the mass-flow rate increases beyond $V_{\text{in}}/V_{\infty} = 0.4$, the C_L/C_D ratio rises steadily, reaching a peak at $V_{\text{in}}/V_{\infty} = 2$. At this point, the performance shows an additional 10% improvement over the clean diffuser.

The improvement in the C_L/C_D ratio can be attributed to the enhanced downforce generation enabled by the active flow implemented with the TVC system. Further analysis of the lift and drag coefficients is presented in Figure 10, the introduction of the TVC results in a maximum increase of approximately 14% in downforce. With increasing mass-flow rate from the blowing slot, the vortex trapped and formed within the cavity. This recirculating vortex, energized by the injected flow inside the cavity, induces a localized suction peak near the stagnation region. Upon exiting the cavity, the high-momentum fluid interacts with the main flow, promoting reattachment along the diffuser surface. This behavior effectively increases the pressure differential across the diffuser, enhancing the negative camber effect. As a result, the diffuser generates progressively greater downforce with increasing mass-flow rate.

The evolution of the pressure coefficient throughout the diffuser, as presented in Figure 11, further supports the effectiveness of the TVC system in enhancing downforce generation. With increasing mass-flow rates introduced through the TVC blowing slot, the pressure distribution exhibits a more pronounced secondary pressure recovery region. Specifically, a second suction peak emerges downstream of the initial low-pressure region near the blowing slot. This indicates the formation of another area of accelerated flow and enhanced pressure drop. Furthermore, a stabilized trapped vortex within the cavity generates an additional suction peak near the TVC stagnation point. This sequence of low-pressure zones along the diffuser surface increases the overall pressure differential, leading to a greater net aerodynamic force acting downward. The ability of the TVC system to induce multiple suction regions and deepen the pressure recovery process demonstrates its effectiveness in enhancing diffuser performance and generating additional downforce, particularly at higher mass-flow rates.

While the TVC system enhances downforce through active flow control, it also introduces a modest increase in overall drag compared to the clean baseline diffuser, as shown in Figure 10. Although drag remains lower at low mass-flow rates, an upward trend is observed beyond $V_{\text{in}}/V_{\infty} = 0.4$, resulting in up to a 4% increase. This increase is primarily attributed to elevated viscous drag caused by the intensified flow exiting the TVC cavity. As high-energy fluid is ejected from the cavity and attaches to the diffuser surface, it energizes the boundary layer along the diffuser wall, increasing shear stress and raising skin friction drag. The strengthened boundary layer attachment contributes positively to flow control but imposes a drag penalty that slightly offsets the overall aerodynamic efficiency, as reflected in the C_L/C_D performance metric.

A performance reduction was observed when a low mass flow rate was applied to the TVC, particularly within the range of $V_{\text{in}}/V_{\infty} < 0.4$. Although the overall performance remains superior to that of a clean diffuser, a slight deterioration in C_L/C_D was noted at the onset of mass flow injection. Specifically, the minimum performance was recorded around $V_{\text{in}}/V_{\infty} \approx 0.4$, followed by a recovery and improvement at higher mass flow rates.

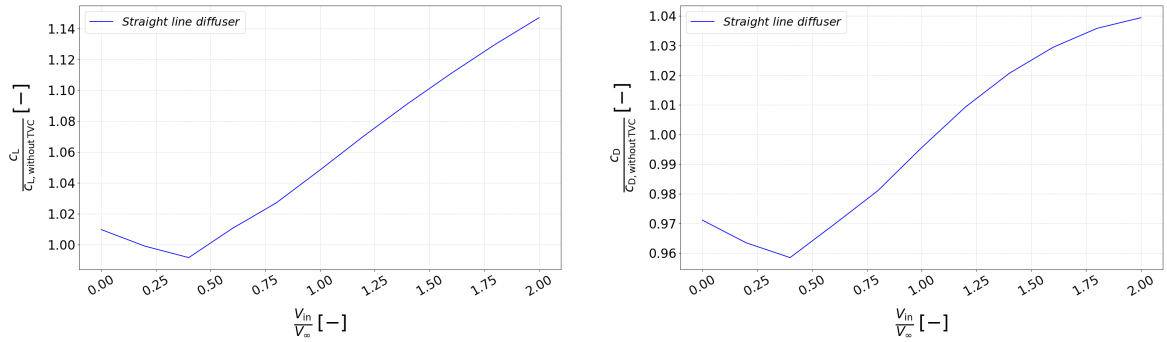

(a) c_L (b) c_D

Figure 10: Straight-line Diffuser attached with TVC at mid location with mass-flow rate anachored inside the cavity: $V_{in}/V_\infty[-]$ represents the mass-flow rate in term of velocity entering into the cavity versus free-stream velocity; $c_L/c_D[-]$ represent Lift coefficient versus Drag coefficient

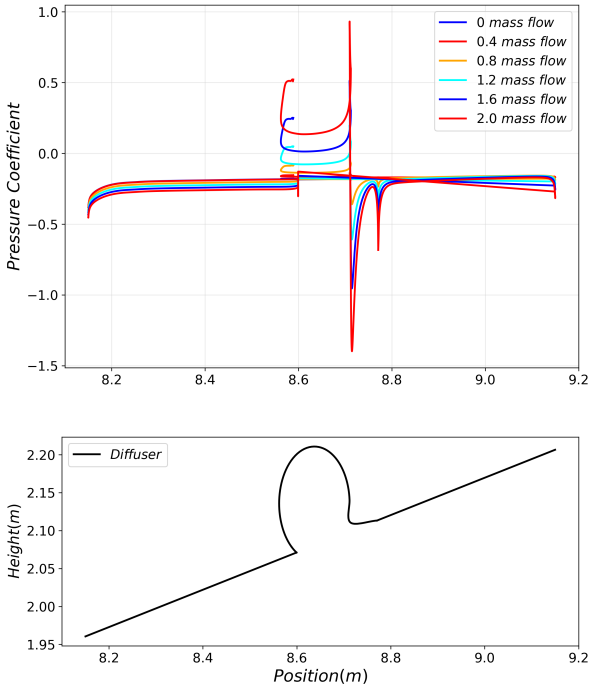

Figure 11: Static pressure plot and the correlated X-axis position for straight-line diffuser attached with TVC at mid location under various mass-flow rates. X-axis represents the diffuser length from inlet to outlet; Pressure coefficient indicates the pressure distribution from the diffuser inlet through the TVC to the outlet.

This initial performance drop can be attributed to the insufficient momentum of the injected flow within the cavity, which fails to maintain effective flow attachment along the rear diffuser wall. Velocity contour plots corresponding to $V_{\text{in}}/V_\infty = 0, 0.2, 0.4$, and 0.6, as shown in Figure 12, illustrate the evolution of this phenomenon. At zero mass flow rate, despite the absence of a well-defined vortex structure within the cavity, the geometry of the TVC appears to energize the surrounding flow, promoting partial reattachment at the rear section of the diffuser.

However, at low but non-zero mass flow rates ($V_{\text{in}}/V_\infty = 0.2$), the injected flow is insufficiently directed and lacks the momentum necessary to remain attached along the diffuser surface. Instead, the flow is deflected downward, disrupting the pressure recovery process and contributing to the underbody flow. As the mass flow rate increases toward $V_{\text{in}}/V_\infty = 0.4$, this deflection becomes more pronounced, with the flow from the TVC being diverted into the underbody region. This adversely affects the pressure gradient near the rear diffuser, as the main flow is entrained toward the underbody, thereby interrupting the diffuser's pressure recovery capability and resulting in a further degradation in C_L/C_D.

At $V_{\text{in}}/V_\infty = 0.6$, a significant improvement in performance is observed. At this threshold, the injected mass flow possesses sufficient energy and directionality to reattach to the rear diffuser surface, thereby re-establishing effective pressure recovery. The enhanced mixing and momentum exchange in this regime contribute to improved aerodynamic efficiency and a subsequent rise in the C_L/C_D ratio.

Moreover, despite the mid-section TVC configuration effectively enhancing suction and generating a secondary low-pressure region, it fails to guide the underbody flow from the diffuser inlet upward along the diffuser surface. As a result, a large wake region persists at the rear of the diffuser, which diminishes its effectiveness in reducing pressure drag. This limits the overall drag-reduction potential of the TVC.

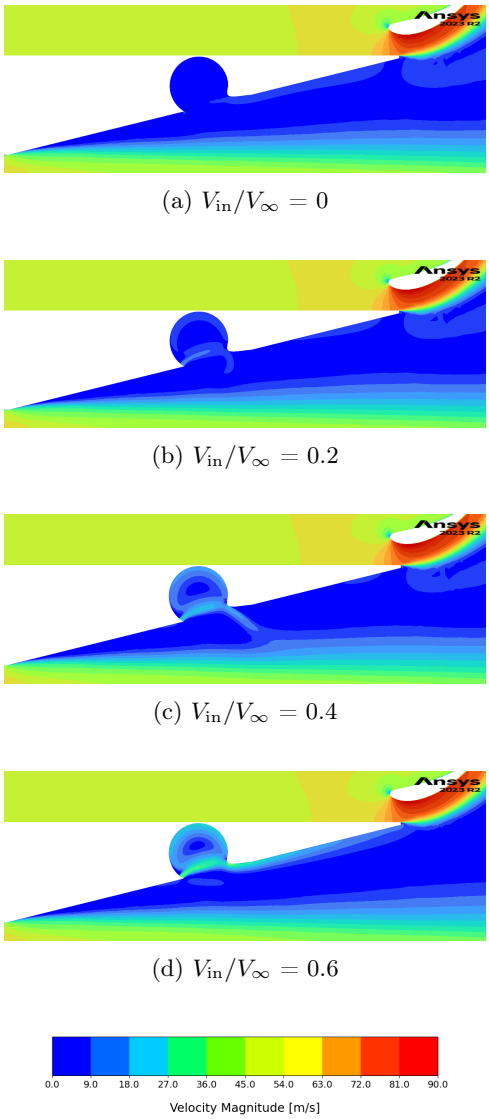

(a) $V_{\text{in}}/V_{\infty} = 0$

(b) $V_{\text{in}}/V_{\infty} = 0.2$

(c) $V_{\text{in}}/V_{\infty} = 0.4$

(d) $V_{\text{in}}/V_{\infty} = 0.6$

Figure 12: Velocity contours of the Straight-line Diffuser with TVC at V_{in}/V_{∞} ratios of 0, 0.2, 0.4, and 0.6. The color bar represents the velocity magnitude.

Although the active TVC system demonstrates an improvement in the C_L/C_D ratio, it operates at the expense of continuous external energy input to maintain vortex trapping and enhance the suction effect. The actual energy cost associated with sustaining the active flow control remains an essential factor and warrants further investigation before such systems can be considered viable for practical applications.

A passive aerodynamic approach has been proposed as an alternative to address the limitations of active flow control. This method introduces a low-drag tunnel that connects the TVC cavity to the freestream, enabling a continuous mass-flow supply solely through geometric modification without needing external energy input. The primary objective of this passive configuration is to maintain stable vortex strength within the cavity to ensure effective vortex trapping while simultaneously avoiding excessive energization of the exit flow. Doing so mitigates the risk of additional viscous drag on the diffuser surface, thereby preserving aerodynamic efficiency without the energy cost associated with active systems.

2. *Passive Aerodynamics Case*

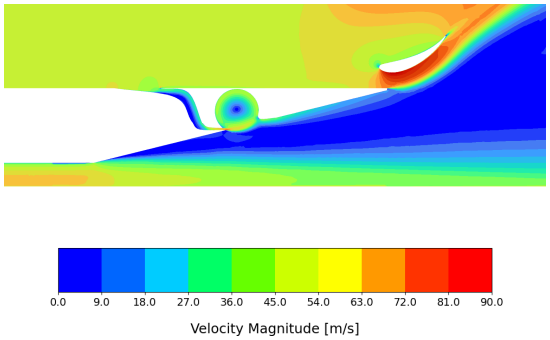

Parameter	Value [-]
$\frac{c_L}{c_{L,\text{without TVC}}}$	1.12
$\frac{c_D}{c_{D,\text{without TVC}}}$	1.037
$\frac{c_L}{c_D} \cdot \frac{c_D}{c_{L\ \text{without TVC}}}$	1.08

Table IV: Velocity contours and aerodynamic performance summary of the passive aerodynamics case.

Table IV illustrates the performance of the TVC system when connected to a low-drag passive blowing channel. The velocity contours indicate that airflow successfully passes through the tunnel and accelerates at the exit, generating a flow strength to trap and stabilize a vortex within the cavity, forming a recirculation region. As a result, a suction peak is intensified near the stagnation point, creating a secondary pressure recovery zone—an effect similar to that observed in the active control case. This tunnel-assisted passive configuration contributes to an additional 12% increase in downforce.

Similar to the energetic flow produced by active flow control, the flow generated by the tunnel is still unable to effectively direct the underbody airflow upward along the diffuser surface. As a result, it induces a drag penalty comparable to that observed in the active flow control case. Additionally, the passive tunnel introduces a small amount of extra drag due to the presence of a localized recirculation region within the tunnel. Despite these limitations, this passive aerodynamic approach—achieved without any external

energy input—still yields an 8% improvement in the C_L/C_D.

C. Airfoil-shaped Diffuser

1. Active Aerodynamics Case - TVC at leading and mid edge of the diffuser

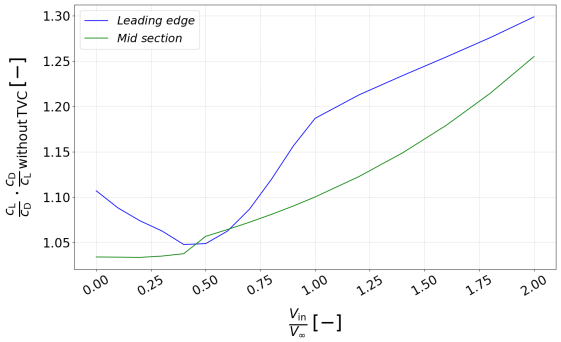

Figure 13: Airfoil-shaped Diffuser attached with TVC applied with mass-flow rate anachored inside the cavity: $V_{in}/V_\infty[-]$ represents the mass-flow rate in term of velocity entering into the cavity versus free-stream velocity; $c_L/c_D[-]$ represent Lift coefficient versus Drag coefficient: Blue line refers to diffuser with TVC located at leading edge, the green line refers to diffuser with TVC located at the mid-section.

Following the baseline diffuser performance discussion, the TVC was introduced into the airfoil-shaped diffuser, as illustrated in Figure 3, to achieve performance enhancement through both passive and active flow control. The TVC was tested at different positions along the diffuser, each selected based on its expected influence. One configuration placed the TVC near the leading edge of the diffuser, in close proximity to the local suction peak region induced by the inlet pumping effect. This placement aimed to amplify the suction effect at the diffuser entrance and enhance the underbody flow interaction. In another configuration, the TVC was positioned at the mid-section of the diffuser, inspired by the previous baseline diffuser case. This setup was intended to generate a secondary pressure recovery region downstream, thereby improving the overall pressure recovery and increasing the diffuser's C_L/C_D.

The results of the two parametric studies are presented in Figure 13. The findings indicate that both TVC placement positions—at the leading edge and mid-section of the diffuser—provide performance improvements compared to the clean airfoil-shaped diffuser across the entire range of mass flow rates, notably, even at zero mass flow, the inclusion of the TVC results in an increase in the C_L/C_D by 10.7% when placed near the leading edge, and by 3.40% when placed at the mid-section. Although a slight reduction in performance is observed at lower mass flow rates, both configurations show significant improvements once the mass flow rate exceeds 0.5. At a mass flow rate of 2.0, the TVC placed at the front of the diffuser yields a 29.8% increase in C_L/C_D, while the mid-positioned TVC achieves a 25.5% improvement.

Although both TVC placements yield significant performance improvements, positioning the TVC near the leading edge of the diffuser results in superior aerodynamic performance compared to placing it at the mid-section. This advantage is primarily attributed to the leading-edge TVC's ability to generate a more substantial suction effect and reduce the size of the wake region more effectively.

The enhanced suction effect from the leading-edge TVC arises from its proximity to the ground and its direct exposure to the high-speed freestream flow entering the diffuser. When placed at the diffuser's front, the cavity interacts with the incoming constrained freestream velocity, allowing a greater volume of high-momentum fluid to be entrained into the cavity. With the assistance of the blowing power from the slot, this configuration facilitates the trapping of a high-energy underbody flow, which amplifies the suction peak near the stagnation point of the cavity. When superimposed with the natural suction effect at the diffuser inlet, this suction peak leads to a more pronounced pressure drop and stronger flow acceleration near the leading edge.

In contrast, the mid-section TVC primarily interacts with the flow that has already been diffused, which is slower and often recirculating. As a result, the volume and energy of the captured flow are reduced, leading to a weaker trapped vortex and lower suction intensity. This is evident in the lift coefficient results shown in Figure 14, where the leading-edge TVC achieves about a 20% increase in downforce at a mass flow rate of 2.0 V_{in}/V_∞, compared to 16.8% for the mid-section TVC.

Furthermore, the leading-edge TVC configuration contributes to a more significant drag reduction. By maximizing the diffuser's effectiveness, the leading-edge TVC helps extend the region of accelerated flow further downstream, thereby reducing the size of the wake. Although the TVC introduces additional viscous drag due to increased surface interaction, this is outweighed

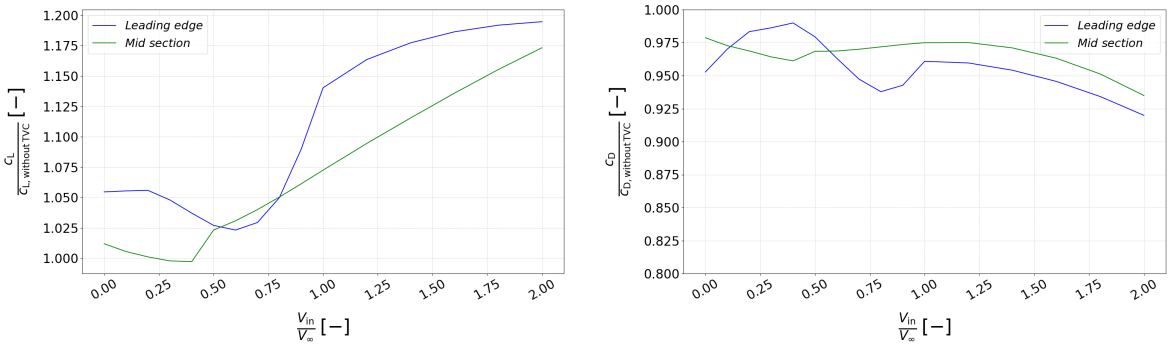

(a) c_L (b) c_D

Figure 14: Airfoil shaped diffuser with TVC at leading and mid edge. V_{in}/V_∞ denotes the velocity ratio of cavity inlet flow to freestream. c_L/c_D represents the lift-to-drag coefficient ratio. Blue line refers to diffuser with TVC located at leading edge, the green line refers to diffuser with TVC located at the mid-section.

by the significant suppression of the separation region. The velocity contours of the diffuser equipped with the TVC system at various mass flow rates are illustrated in Figure 15, once the cavity mass flow ratio exceeds 1.6 V_{in}/V_∞, the flow exiting the cavity remains fully attached to the diffuser surface. This re-energized underbody flow merges with the diffuser boundary layer, reducing the extent of the wake region compared to the clean diffuser case.

While the mid-section TVC also energizes part of the wake, its downstream position leaves a portion of the wake region unaffected, particularly between the inlet and the cavity. Consequently, the drag reduction is less substantial compared to the leading-edge configuration. This trend is confirmed by the drag coefficient data in Figure 14, where the leading-edge TVC consistently achieves more significant drag reduction, particularly beyond $V_{\text{in}}/V_\infty = 0.8$, as it begins to expand and energize the underbody flow field significantly.

Thus, it is evident that the TVC placed at the leading edge of the diffuser effectively leverages the underbody flow, leading to a marked improvement and providing direction for future optimization of the diffuser's performance.

2. *Active Aerodynamics Case - TVC with diameters variation*

The following parametric study investigates the aerodynamic performance of a diffuser with an active TVC located at its leading edge, with varying TVC diameter ratios. The diameter ratio is defined as $D_{\text{TVC}}/L_{\text{diff}}$, where D_{TVC} is the diameter of the TVC and L_{diff} is the length of the diffuser's ramp surface. The results, shown in Figure 16, present the C_L/C_D performance for diameter ratios ranging from 0.165 to 0.185. The upper limit of 0.185 is imposed by geometric constraints, representing the maximum allowable TVC diameter at the diffuser inlet.

The data reveal a consistent trend across all diameter ratios: the C_L/C_D ratio increases with the rising mass-flow rate. At higher mass-flow rates (above $V_{\text{in}}/V_\infty = 1.2$), the performance difference between diameter ratios becomes more pronounced. Larger $D_{\text{TVC}}/L_{\text{diff}}$ values contribute to higher C_L/C_D performance, with the maximum observed at a ratio of 0.185. At this condition, a performance improvement of approximately 10% is achieved compared to the smallest tested ratio of 0.165.

The static pressure contours for each diameter ratio, evaluated at a mass-flow rate of $V_{\text{in}}/V_\infty = 2.0$ and presented in Figure 17, provide further insight into the aerodynamic behavior of the TVC system. In all cases, a region of low static pressure forms consistently near the TVC exit. As the cavity diameter increases, the static pressure near the stagnation point decreases further. This indicates that, under high mass-flow conditions, a larger TVC diameter intensifies the suction effect by generating a lower static pressure region. This enhanced suction increases downforce and strengthened the local suction peak near the diffuser inlet, improving the C_L/C_D ratio. These observations explain the superior aerodynamic efficiency associated with larger diameter ratios.

3. *Passive Aerodynamics Case*

The contour plot shown in Table V illustrates the aerodynamic performance of the passive TVC

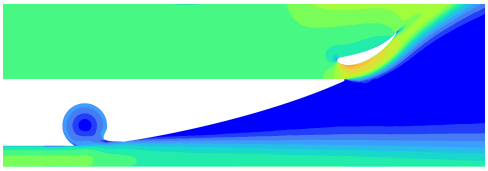

(a) $V_{in}/V_{\infty} = 0$

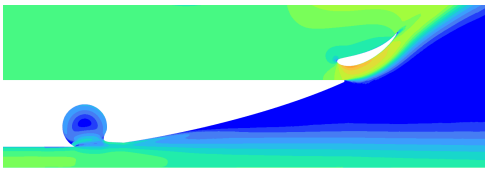

(b) $V_{in}/V_{\infty} = 0.8$

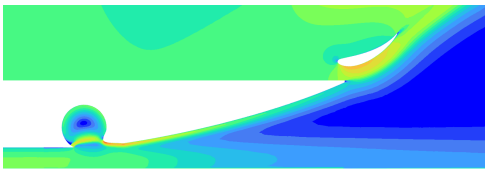

(c) $V_{in}/V_{\infty} = 1.6$

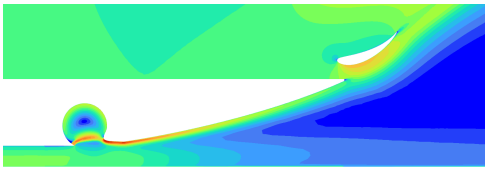

(d) $V_{in}/V_{\infty} = 2.0$

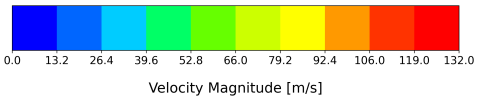

Figure 15: Velocity contours of the Airfoil-shaped Diffuser with TVC at V_{in}/V_{∞} ratios of 0, 0.8, 1.6, and 2.0. The color bar represents the velocity magnitude.

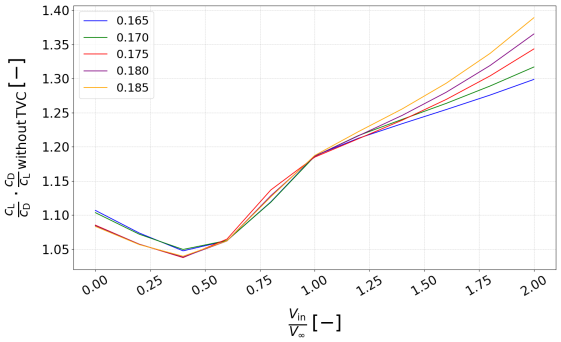

Figure 16: Airfoil-shaped Diffuser attached with TVC with different radius variation: The diameter of each TVC is represent as D_{TVC}/L_{diff} : D_{TVC} represents the diameter of TVC; L_{diff} represents the length of diffuser

(a) $D_{TVC}/L_{diff} = 0.165$

(b) $D_{TVC}/L_{diff} = 0.170$

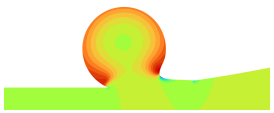

(c) $D_{TVC}/L_{diff} = 0.175$

(d) $D_{TVC}/L_{diff} = 0.180$

(e) $D_{TVC}/L_{diff} = 0.185$

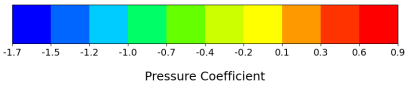

Figure 17: Pressure contours for different diameter-to-diffuser length ratios D_{TVC}/L_{diff} at mass flow rate of 2.0 V_{in}/V_{∞}.

configuration. This setup follows the geometric settings of the straight-line diffuser case and builds upon the previous findings from the active method analysis. In the passive configuration, a low-drag tunnel is connected to the TVC placed at the leading edge of the diffuser, aiming to improve C_L/C_D performance without requiring additional power input.

The performance data, also presented in Table V, indicate that the passive method achieves a 27% increase in downforce despite incurring a 2.7% drag penalty. Overall, this results in a 23.6% improvement in C_L/C_D compared to the baseline airfoil-shaped diffuser without a TVC or blowing channel.

The superior performance of the passive configuration can be primarily attributed to its enhanced downforce generation. With its inlet exposed to the freestream, the tunnel successfully induces a strong suction effect and accelerates the airflow at its outlet. This acceleration sustains a sufficiently high mass-flow rate into the cavity, promoting the entrainment of underbody flow and maintaining a strong vortex structure. The increased vortex

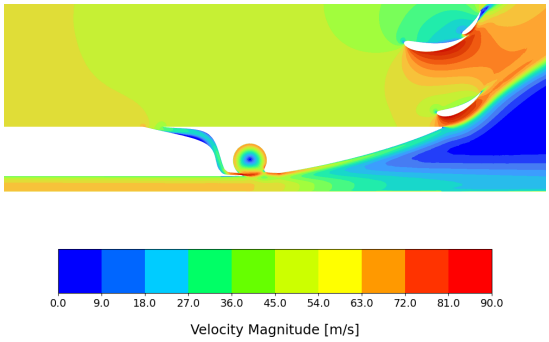

Parameter	Value [-]
$\frac{c_L}{c_{L,\text{without TVC}}}$	1.270
$\frac{c_D}{c_{D,\text{without TVC}}}$	1.027
$\frac{c_L}{c_D} \cdot \frac{c_D}{c_{L\text{ without TVC}}}$	1.236

Table V: Velocity contours and aerodynamic performance summary of the passive aerodynamics case.

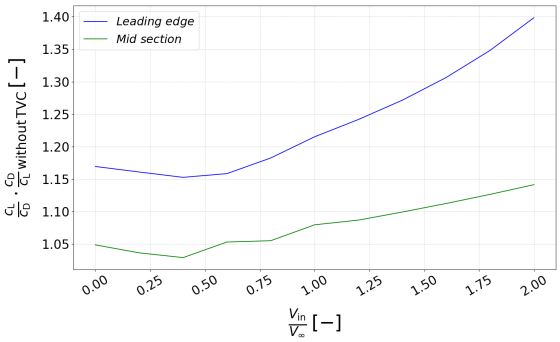

Figure 18: Formula one Diffuser attached with TVC applied with mass-flow rate anachored inside the cavity: $V_{in}/V_\infty[-]$ represents the mass-flow rate in term of velocity entering into the cavity versus free-stream velocity; $c_L/c_D[-]$ represent Lift coefficient versus Drag coefficient: Blue line refers to diffuser with TVC located at leading edge, the green line refers to diffuser with TVC located at the mid-section.

strength enhances the suction effect near the cavity's stagnation point, thereby boosting downforce.

Additionally, the curved design of the inverted airfoil facilitates greater flow acceleration at the outlet compared to the straight-line configuration. This helps the flow remain attached along the diffuser surface, effectively increasing the camber effect and further enhancing downforce.

Another contributing mechanism to the downforce, comparable to the active configuration, is the pressure differential generated across the tunnel. As the airflow re-accelerates through the tunnel, a low-pressure region forms near the outlet. This creates a static pressure difference between the ambient-pressure inlet and the low-pressure outlet, resulting in an adverse pressure force that acts downward on the diffuser. On the other hand, the constrained underbody flow generates a lower static pressure region near the tunnel outlet. This low-pressure region enhances suction at the tunnel entrance, resulting in more effective tunnel airflow compared to the configuration with the TVC placed at the mid-section of the diffuser, as shown in Table IV. Although this enhanced downforce introduces a 2.7% drag penalty—primarily due to viscous effects—the overall aerodynamic efficiency, measured by C_L/C_D, still improves by 23.6%.

D. Formula one inspired Diffuser

1. *Active Aerodynamics Case - TVC at leading and mid edge of the diffuser*

The C_L/C_D performance comparison between TVC located at the leading edge and the mid-section of a contemporary Formula one diffuser is presented in Figure 18. The results demonstrate a consistent improvement in aerodynamic efficiency for both locations. At zero mass-flow rate ($V_{\text{in}}/V_\infty = 0$), the leading-edge configuration yields a 17% improvement in C_L/C_D, while the mid-position yields a 5% improvement. With increasing mass-flow rates, both configurations show steady performance gains. At $V_{\text{in}}/V_\infty = 2.0$, the leading-edge TVC achieves an enhancement of approximately 40%, while the mid-position achieves a 14% improvement in C_L/C_D.

Although both configurations benefit from increased mass-flow rates, placing the TVC closer to the diffuser inlet demonstrates superior aerodynamic performance. This advantage is primarily attributed to more effective drag reduction, as demonstrated by the plot of the lift and drag coefficients of the diffuser with TVC at the leading and mid-edges, shown in Figure 19. The drag for the leading-edge TVC configuration is continuously reduced with increasing flow rate, reaching a reduction of up to 20% compared to the baseline Formula one diffuser without TVC. In contrast, the mid-position configuration exhibits oscillatory drag behavior and does not achieve significant drag reduction.

This performance difference can be attributed to the specific curvature design of the Formula one diffuser. The front-mid section of the diffuser features a slightly concave surface, which tends to generate a larger wake region. The presence of a substantial wake region increases pressure drag. When the TVC is placed at the leading edge, it traps the underbody flow and directs high-energy

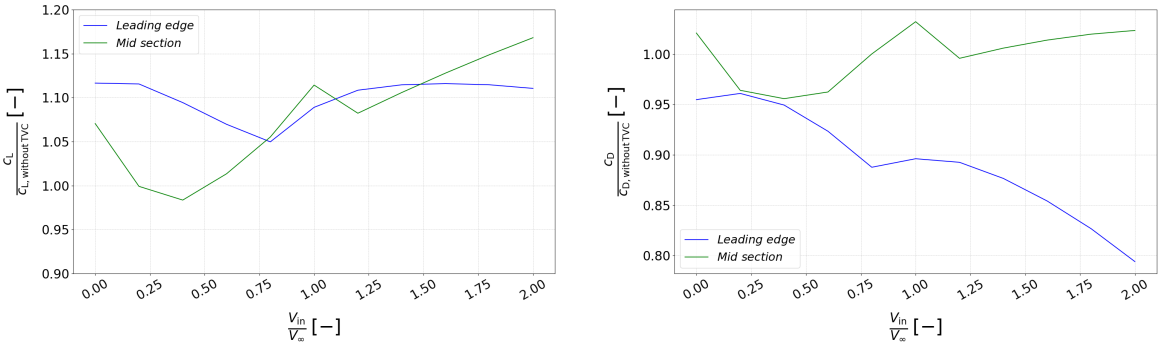

(a) c_L (b) c_D

Figure 19: Formula one diffuser with TVC at leading and mid edge. V_{in}/V_∞ denotes the velocity ratio of cavity inlet flow to freestream. c_L/c_D represents the lift-to-drag coefficient ratio. Blue line refers to diffuser with TVC located at leading edge, the green line refers to diffuser with TVC located at the mid-section.

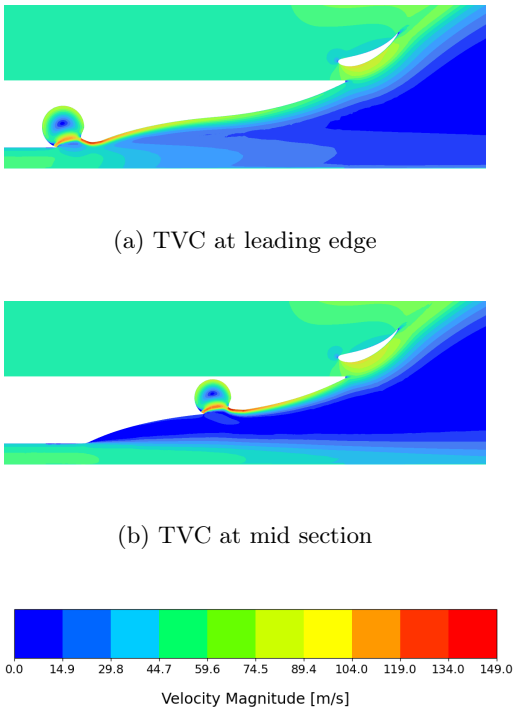

(a) TVC at leading edge

(b) TVC at mid section

Figure 20: Velocity contours of the Formula one Diffuser with TVC at V_{in}/V_∞ ratios of 2.0.

airflow upward into the concave region. This re-energized flow remains attached to the diffuser surface, reducing the wake region and thereby decreasing drag. Conversely, when the TVC is placed at the mid-section, it energizes the flow only in the latter part of the diffuser. This leaves the flow in the upstream region (from the diffuser inlet to the TVC) largely unaffected, as displayed in the velocity contours in Figure 20, resulting in a persistently large wake region and limited drag reduction.

On the other hand, while the mid-position TVC is less effective at reducing drag, it provides superior downforce generation at higher mass-flow rates. This becomes particularly evident at $V_{\text{in}}/V_\infty = 2.0$, where the mid-position configuration produces 5.8% more downforce than the leading-edge counterpart ,as shown in Figure 19.

The difference in downforce performance is also attributed to the diffuser's curvature. Unlike the concave shape in the front-mid section, the mid-end section of the diffuser incorporates a convex curvature. This geometry causes the ejected airflow from the TVC to undergo a sharper turning motion, which accelerates the flow and lowers the static pressure in the region between the cavity exit and the diffuser surface. In contrast, the rounded geometry at the leading edge results in a milder acceleration of the ejected flow, producing a comparatively weaker suction effect. Although the leading-edge TVC still traps a substantial amount of underbody flow, its capacity to enhance downforce at higher mass-flow rates further is limited due to this geometric constraint.

A comparison of the static pressure distribution of the TVC system, with placements at the leading edge and the mid-section, is presented in Figure 21. The mid-position TVC configuration generates a notably lower static pressure region than the leading-edge configuration. This indicates a more substantial suction effect, correlating with the observed increase in downforce.

In conclusion, the performance of the TVC is strongly influenced by the strength of the diffuser underbody flow and the surface curvature. When placed near the diffuser inlet, the TVC—especially with an applied blowing slot—can enhance the suction peak and reduce wake region size, leading to

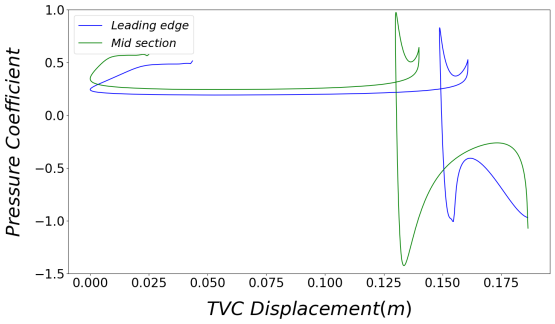

Figure 21: Static Pressure of TVC located at two location under the same displacement for comparsion: Blue line refers to diffuser with TVC located at leading edge, the green line refers to diffuser with TVC located at the mid-section.

significant drag reduction. Additionally, placement on sharper surfaces promotes a lower static pressure region at the cavity exit, further improving suction effects. To identify the optimal C_L/C_D performance, the following analysis will focus on configurations with the TVC positioned at the front of the diffuser.

2. *Active Aerodynamics Case - Cases comparsion between Airfoil-shaped Diffuser and Formula one inspired diffuser*

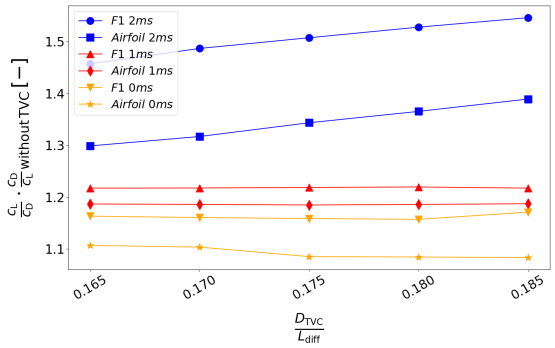

Figure 22: Performance comparison between the Formula One diffuser and the airfoil-shaped diffuser, with each TVC configuration normalized to its respective baseline diffuser without TVC.

Combined with Figure 16, the plot in Figure 22 illustrates the relative aerodynamic performance of TVC-equipped configurations for both Formula One and airfoil-shaped diffusers, evaluated over the same range of TVC diameters. Each curve is normalized to its respective baseline (no-TVC) configuration. The normalization allows the comparison to focus primarily on the improvement rate introduced by the TVC geometry, enabling a more precise evaluation of its effectiveness across different diffuser geometries.

The analysis of Figure 22 reveals that even at zero mass-flow rate input, the implementation of the TVC still results in a 10% to 12% improvement in C_L/C_D across all $D_{\text{TVC}}/L_{\text{diff}}$ values. Further improvements are observed at higher mass-flow rates. When $V_{\text{in}}/V_\infty \geq 1$, both diffuser geometries consistently exhibit enhanced performance across all TVC diameter ratios. This suggests that the injected momentum from the TVC flow plays an increasingly dominant role in energizing the diffuser suction peak and improving flow attachment as the mass-flow rate increases. Particularly, the benefits of larger TVC diameters become more pronounced under these higher mass-flow conditions. At the largest tested diameter ratio ($D_{\text{TVC}}/L_{\text{diff}} = 0.185$) and the largest mass-flow rate of $V_{\text{in}}/V_\infty = 2$, the airfoil-shaped diffuser achieves a 38.9% improvement in C_L/C_D, while the Formula One diffuser achieves a notable 54.6% improvement. This performance gain can be attributed to the stronger suction peak near the cavity stagnation point. The larger TVC radius helps anchor a more stable and intense vortex within the cavity, accelerating the internal flow and enhancing the suction effect, ultimately improving the overall aerodynamic performance.

Additionally, the TVC system consistently performs better in the Formula One diffuser than in the airfoil-shaped diffuser for all TVC diameter ratios and mass-flow conditions. This advantage is primarily due to the greater drag reduction achieved in the Formula One diffuser, which stems from its more concave geometry. As shown in Figure 23, the baseline (no-TVC) Formula One diffuser generates a larger wake region compared to the airfoil-shaped diffuser due to its stronger curvature and associated adverse pressure gradient. However, when TVC is applied with the same radius and mass-flow rate, the resulting wake regions in both diffusers are significantly reduced and become visually comparable in size. This indicates that the TVC reduces a larger portion of the wake in the Formula One diffuser, leading to a more substantial drag-reducing effect and, thus, a greater enhancement in C_L/C_D performance.

3. *Passive Aerodynamics Case*

Table VI demonstrates the aerodynamic effectiveness of incorporating a passive tunnel connected to a TVC system at the leading edge of the diffuser. The TVC geometry used in this configuration is similar to that employed in the airfoil-shaped diffuser case shown in Table V.

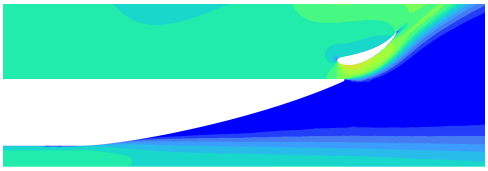

(a) Original Airfoil shaped diffuser

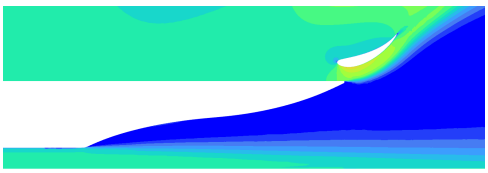

(b) Original Formula one diffuser

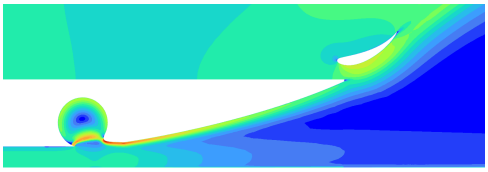

(c) TVC at airfoil-shaped diffuser, with mass-flow rate $V_{\text{in}}/V_{\infty} = 2$

(d) TVC at Formula one diffuser, with mass-flow rate $V_{\text{in}}/V_{\infty} = 2$

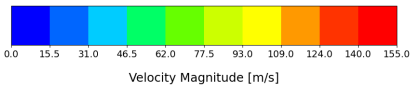

Figure 23: Velocity contours of the Airfoil shaped diffuser and Formula one Diffuser.

The results indicate that introducing the passive tunnel leads to a 12.8% improvement in performance in C_L/C_D compared to the clean Formula One diffuser without TVC. Specifically, the passive method contributes to an 8% increase in downforce while simultaneously achieving a 5% reduction in drag.

Although the downforce improvement is positive, it is less significant than that observed in the airfoil-shaped diffuser with a passive tunnel. This difference can be attributed to the distinct flow acceleration characteristics as the flow exits

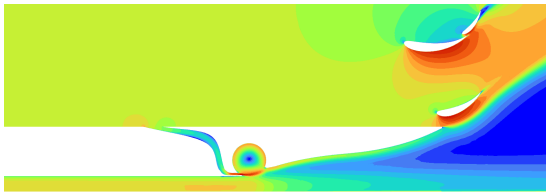

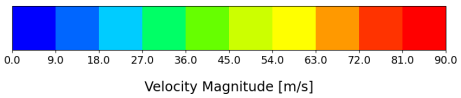

Parameter	Value [-]
$\frac{c_L}{c_{L,\text{without TVC}}}$	1.08
$\frac{c_D}{c_{D,\text{without TVC}}}$	0.95
$\frac{c_L}{c_D} \cdot \frac{c_D}{c_{L\text{ without TVC}}}$	1.129

Table VI: Velocity contours and aerodynamic performance summary of the passive aerodynamics case.

the cavity. In the airfoil-shaped diffuser, the flow is forced to follow the sharp curvature of the inverted airfoil leading edge, undergoing a rapid turning motion and reattachment to the diffuser surface. This sharp turn induces additional flow acceleration, enhancing the suction effect and increasing downforce. In contrast, the Formula One diffuser features a more rounded geometry near the leading edge. As a result, the ejected flow experiences a gentler transition, with reduced acceleration and a weaker suction effect, leading to a minor contribution to downforce generation compared to the airfoil-shaped case.

Nevertheless, the passive TVC tunnel's placement effectively reduces drag. Trapping and redirecting the underbody flow helps to energize the wake region near the diffuser exit, thereby mitigating flow separation and lowering pressure drag. This mechanism explains the observed drag reduction associated with the passive tunnel configuration in the Formula One diffuser.

E. Performance Comparison Across Three Diffuser Configurations

To summarize the findings discussed in the previous sections, Figure 24 presents a comparative analysis of the aerodynamic performance of the TVC across the three diffuser configurations. The comparison is based on cases with an equal ratio of $D_{\text{TVC}}/L_{\text{diff}}$, aiming to identify the most effective TVC placement location and diffuser curvature for maximizing the C_L/C_D ratio. Additionally, a supplementary case featuring a TVC placed at the leading edge of the straight diffuser is included to enable a more comprehensive comparison.

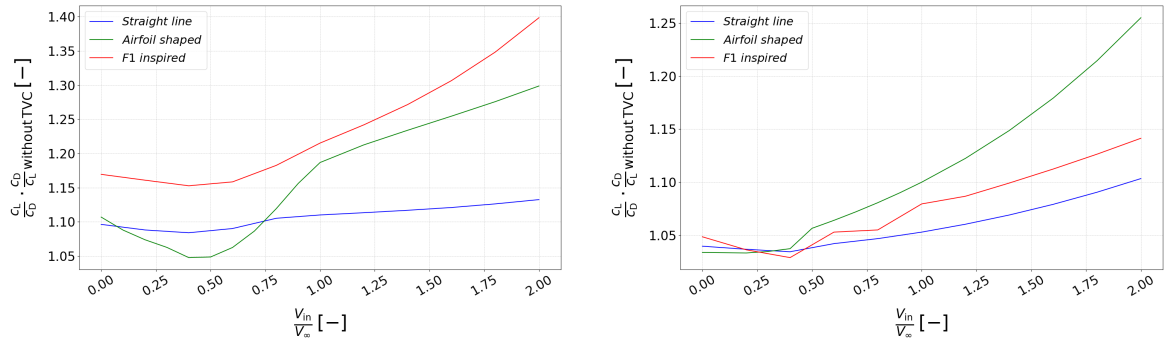

(a) Leading edge

(b) Mid section

Figure 24: Performance comparison across three diffuser configurations with TVC applied at the leading edge and mid-section. Each TVC configuration is normalized relative to its corresponding baseline diffuser without TVC.

By comparing the placement locations, it is observed that TVC positioned at the leading edge consistently outperforms mid-section placement across all three diffuser configurations. This result suggests that enhancing the localized suction peak near the diffuser inlet provides greater aerodynamic efficiency than inducing a secondary low-pressure region during the pressure recovery process. The leading-edge placement effectively traps high-energy underbody flow near the diffuser inlet, thereby maximizing the diffuser's expansion capability. This mechanism contributes to reducing the size of the wake region at the vehicle's rear. In contrast, mid-section placement lacks the ability to capture underbody flow early in the diffuser, often resulting in an unchanged wake region size and, consequently, lower drag reduction efficiency. This leads to a less favorable C_L/C_D compared to the leading-edge configuration.

Despite reduced drag reduction when placed at the mid-section, the TVC still delivers notable performance improvements relative to the clean diffuser. In particular, the airfoil-shaped diffuser achieves a maximum improvement of up to 25%. As discussed in the previous section, this enhancement is attributed to the TVC's ability to promote a secondary pressure recovery point. The blowing slot within the cavity enhances internal flow dynamics, resulting in a localized region of lower static pressure at the cavity outlet, which intensifies with increasing mass-flow rate. This mechanism contributes to additional downforce generation, ultimately improving the overall aerodynamic performance as reflected in a higher C_L/C_D ratio.

Curvature also plays a critical role in determining the efficiency of the TVC system. Among the three configurations, placing the TVC at the leading edge of the Formula One-inspired diffuser yields the highest C_L/C_D ratio, with an improvement of approximately 40%. This superior performance can be attributed to the concave curvature at the front section of the Formula One-inspired diffuser, which, as previously discussed, contributes significantly to pressure drag generation. When the TVC is positioned at the leading edge, it enhances the diffuser's expansion capability, energizing the underbody flow and reducing the wake region size in the aft section. This results in substantial drag reduction and improved aerodynamic efficiency. In contrast, the straight-line diffuser exhibits the least improvement. Due to its minimal curvature, it produces a weaker camber effect on the ejected airflow, resulting in less effective flow attachment and limited diffuser expansion. Consequently, the aerodynamic benefits from the TVC are diminished in this configuration.

However, when the TVC is placed at the mid-section, a different trend is observed. The airfoil-shaped diffuser outperforms the Formula One-inspired diffuser at the same mid-location, achieving a C_L/C_D improvement of approximately 25% compared to 14%. This difference is attributed to the sharper corner geometry adjacent to the TVC exit in the mid-section of the airfoil-shaped diffuser. This sharper curvature promotes more abrupt turning of the ejected airflow, enabling greater flow acceleration. As discussed earlier, the mid-section improvement is driven by the formation of a secondary low-pressure region. The accelerated flow intensifies this effect, further lowering static pressure downstream and enhancing downforce generation. Although the Formula One-inspired diffuser also features a mild convex curvature near its aft region—yielding better performance than the straight-line configuration—it provides a less pronounced turning surface compared to the airfoil-shaped design. As a result, its ability to accelerate the ejected

flow and induce a strong secondary suction effect is reduced, along with a larger wake region unsolved in the frontal section of the diffuser, leading to a less competitive C_L/C_D enhancement.

As illustrated by the combined results presented in Figure 24, both TVC placement and diffuser curvature design play critical roles in determining TVC effectiveness. Positioning the TVC at the leading edge generally yields superior drag reduction, while mid-section placement can also deliver substantial aerodynamic benefits, primarily through enhanced downforce generation. Overall, the configuration featuring the TVC at the leading edge of the Formula One-inspired diffuser achieves the most optimal performance in terms of C_L/C_D.

V. CONCLUSION

This study investigated the effectiveness of the TVC concept, incorporating both active and passive flow control methods across various diffuser geometries using numerical simulations. The results demonstrated a significant improvement in the C_L/C_D across all diffuser types studied. This enhancement is primarily attributed to the strong ejection flow from the TVC cavity, which generates a suction effect at the cavity exit. The resulting suction interacts with the underbody flow, increasing the suction peak along the diffuser surface compared to the baseline configurations.

For active flow control, placing the TVC at the mid-section of the straight diffuser resulted in a 10% increase in C_L/C_D. For the airfoil-shaped and Formula One-inspired diffusers, leading-edge TVC placement with a cavity length ratio of $D_{\mathrm{TVC}}/L_{\mathrm{diff}} = 0.185$ led to improvements of 38.9% and 54.6%, respectively.

For passive flow control, all diffuser types showed performance gains despite the absence of external energy input. The straight diffuser achieved an 8% improvement with mid-section tunnel placement, while the airfoil-shaped and Formula One-inspired diffusers recorded gains of 23.6% and 12.9%, respectively.

The results demonstrate that the TVC system, under active flow control, performs effectively not only in the front wing but also in diffusers. This suggests that the TVC mechanism can be successfully integrated into the aft section of ground vehicles. Furthermore, although passive flow control methods were shown to be less effective in the front wing [1], the current study reveals that even a sub-optimally designed passive tunnel can yield a measurable improvement in C_L/C_D. This highlights the potential for both active and passive TVC implementations to enhance aerodynamic performance in diffuser systems.

The investigation on the effect of TVC placement along the diffuser surface suggests that positioning the TVC at the leading edge yields the most favorable aerodynamic performance. Although placing the TVC at the mid-section can create a secondary low-pressure region, it is less effective at energizing the entire underbody flow, resulting in reduced drag reduction compared to the leading-edge configuration.

Furthermore, the effectiveness of the TVC is shown to be closely related to the diffuser's curvature. When located near sharper ramps, the cavity generates a stronger suction effect, enhancing downforce generation.

This study lays the groundwork for further exploration of the TVC concept. However, the domain used in the present study focuses solely on diffuser performance and includes certain limitations. Specifically, the inlet velocity was set uniformly at 50 m/s for both the upper and lower surfaces, which does not accurately represent the inflow conditions of the real world. Therefore, future work is planned to extend the analysis through high-fidelity, unsteady simulations—such as LES, DDES, and fully three-dimensional modeling—to capture the complex vortex structures and their interactions along the ramp surface and the upper bodywork under more realistic flow conditions. Additionally, the performance of the TVC under disturbed (dirty) air, such as during overtaking scenarios, presents a promising area for investigation. When combined with previous studies on TVC applications on front wings, this research could form a solid foundation for the development of more advanced, efficient aerodynamic strategies in motorsport and high-performance vehicle design.

DATA AVAILABILITY STATEMENT

All data supporting this study are included within this paper.

[1] Ng, M.K. and Teschner, T.-R., "On the Application of Trapped Vortices in Motorsport Application for Improved Aerodynamic Performance Using Passive and Active Flow Controls," SAE Technical Paper 2025-01-5029,2025, DOI: 10.4271/2025-01-5029.

[2] Steinfurth, B, Feldhus, S.,Berthold, A., Haucke, F "Influence of Head Restraint Size on the Aerodynamic Performance of a Formula Student Open-Wheel Race Car" SAE Technical Paper 2018-01-0724, 2018, DOI: 10.4271/2018-01-0724.

[3] Guerrero, A.; Castilla, R, "Aerodynamic Study of the Wake Effects on a Formula 1 Car" Energies 13, no. 19: 5183, 2020, DOI: 10.3390/en13195183.

[4] Crowther, W.J., Jabbal, M., and Liddle, S.C., "Flow Control Fallacies: a Review of Common Pitfalls in Flow Control Research," Journal of Aerospace Engineering, Vol. 225, No. 1, pp. 1-11, 2011, DOI: 10.1243/09544100JAERO761.

[5] Katz J, "Aerodynamics in motorsports," Proceedings of the Institution of Mechanical Engineers, Part P. 2019;235(4):324-338, 2019, DOI: 10.1177/1754337119893226.

[6] Szudarek, M.; Piechna, A.; Piechna, J., "Feasibility Study of a Fan-Driven Device Generating Downforce for Road Cars," Energies 15, no. 15: 5549, 2022, DOI: 10.3390/en15155549.

[7] Dimastrogiovanni M, Reina G, Burzoni A "An improved active drag reduction system for formula race cars"Proceedings of the Institution of Mechanical Engineers, Part D;234(5):1460-1471, 2019, DOI: 10.1177/0954407019862913

[8] Wiegand, Brian "COLIN CHAPMAN and AUTOMOTIVE MASS PROPERTIES, Rev.A" SAWE Paper No.3640, 2022, Page 49

[9] Huminic, Angel and Huminic, Gabriela., "Computational Study Of Curved Underbody Diffusers,"E3S Web of Conferences. 128. 10002, 2019, DOI: 10.1051/e3sconf/201912810002.

[10] Chatpattanasiri, C. ., Bunpapong, K. ., Sahastharachai, M. ., and Puangkird, B., "Numerical study and design of side-diffusers for formula-SAE car,"Journal of Research and Applications in Mechanical Engineering, 10(1), JRAME–22, 2022, DOI: 10.14456/jrame.2022.1

[11] Kuya, Y., Takeda, K., and Zhang, X., "Flow Physics of a Race Car Wing With Vortex Generators in Ground Effect," Journal of Fluid Engineering, Vol. 131, No. 12, 2009, DOI: 10.1115/1.4000423.

[12] Porcar, Laura and Toet, Willem and Gamez-Montero, Pedro, "Study of the Effect of Vertical Airfoil Endplates on Diffusers in Vehicle Aerodynamics," Designs. 5. 45, 2021, DOI: 10.3390/designs5030045.

[13] Kevin M. Peddie,Luis F. Gonzalez, "CFD Analysis of the Diffuser of a Formula 3 Racecar," Orbit,Vol. 1 No. 1, 2009.

[14] Ehirim, O.H., Knowles, K., and Saddington, A.J., "A Review of Ground-Effect Diffuser Aerodynamics," ASME Journal of Fluids Engineering, Vol. 141, Issue. 2, 020801, 2018, DOI: 10.1115/1.4040501.

[15] Ringleb, F.O., "Separation Control by Trapped Vortices," Boundary Layer and Flow Control, ed. G. V. Lachman, Pergamon Press, 1961.

[16] Tutty, O.R., Buffoni, M., Kerminbekov, R., Donelli, R., De Gregorio, F., and Rogers, E., "Control of Flow with Trapped Vortices: Theory and Experiments," International Journal of Flow Control, Vol. 5, No. 2, pp. 89-109, 2013, DOI: 10.1260/1756-8250.5.2.89.

[17] Lasagna, D., Donelli, R., De Gregorio, F., and Iuso, G., "Effects of a Trapped Vortex Cell on a Thick Wing Airfoil," Experiments in Fluids, Vol. 51, No. 5, pp. 1369-1384, 2011, DOI: 10.1007/s00348-011-1160-9.

[18] Panigrahi, C., Chawla, R., and Nair, M.T., "Optimisation of Trapped Vortex Cavity for Airfoil Separation Control," Journal of Applied Fluid Mechanics, Vol. 15, No. 1, pp. 179-191, 2021, DOI: 10.47176/jafm.15.01.32684.

[19] Donelli, R.S., De Gregorio, F., and Iannelli, P., "Flow Separation Control by Trapped Vortex," 48th AIAA Aerospace Sciences Meeting, Paper 2010-1409, 2010, DOI: 10.2514/6.2010-1409.

[20] "Suzuka F1 Circuit Layout and Records," F1 Fansite, https://www.f1-fansite.com/f1-circuits/suzuka-circuit/, accessed Nov. 2024.

[21] "Silverstone F1 Circuit Layout and Records," F1 Fansite, https://www.f1-fansite.com/f1-circuits/silverstone-circuit/, accessed Nov. 2024.

[22] Prince, S.A., Khodagolian, V., Singh, C., and Kokkalis, T., "Aerodynamics Stall Suppression on Airfoil Sections Using Passive Air-Jet Vortex Generators," AIAA Journal 47, no. 9 (2009): 1985-2270, doi:https:// doi.org/10.2514/1.41986.

https://dspace.org/

Enhancing the aerodynamic performance of diffusers in high-performance vehicles using trapped vortex cavities

Ng, Ming Kin; Teschner, Tom-Robin

2026-04-09
Society of Automotive Engineers (SAE)
https://doi.org/10.4271/2026-01-5027
Ng MK, Teschner T-R. (2026) Enhancing the aerodynamic performance of diffusers in high-performance vehicles using trapped vortex cavities. SAE Technical Paper Series, April 2026, Article number 5027

Downloaded from a DSpace repository. https://dspace.org/